Advanced Composites and Hybrid Materials (2021) 4:286–293
https://doi.org/10.1007/s42114-021-00235-y

ORIGINAL RESEARCH

Immobilization of graphitic carbon nitride on wood surface via chemical crosslinking method for UV resistance and self-cleaning

Bingnan Yuan[1,2] · Minghui Guo[1] · Vignesh Murugadoss[3] · Gang Song[4] · Zhanhu Guo[2]

Received: 15 December 2020 / Revised: 27 February 2021 / Accepted: 5 March 2021 / Published online: 11 March 2021

Abstract

To protect the wood surface from UV aging and give it new functions, in this research, graphitic carbon nitride (g-C_3N_4) was firmly immobilized on wood surface via chemical crosslinking method with glutaraldehyde as agent. By constructing the organic-inorganic composite coating between wood and g-C_3N_4, the wood surface was endowed with the functions of UV resistance and self-cleaning. According to the UV-Vis absorption spectra, the g-C_3N_4 coatings could absorb about 85% UVA and UVB lights. The UV resistance properties of the resulting g-C_3N_4-treated wood (GW) were evaluated through 15-day accelerated weathering tests. The surface total color change (ΔE^*) of GW was estimated to be 8%, which was much less than that of original wood (24%). The photocatalytic tests showed that the wood surface could be self-cleaned by the photodegradation of organics on the surface. After 10-cycle photocatalytic activity tests, the remained content of g-C_3N_4 was stable at 84%, which was much higher than the 40% of control group (our reported hydrothermal method). In addition, the water contact angle of wood surface was improved from 55.1° to 78.5°. Overall, these findings look promising for enhancing the service life of wood materials and conservation of wooden artifacts. The obtained functional woods could be used for the development of durable, multi-functional, and environment-friendly wood products.

Keywords Composite · Wood · Graphitic carbon nitride · UV resistance · Functionalization

1 Introduction

Functional coatings have been used on the surfaces of various materials to enhance their properties or endow new functions [1–8]. Wood is a natural organic polymer extensively studied due to its several properties, such as renewability, environment-friendliness, and reusable properties. However, due to its biological features, wood furniture and products are perishable and easy to be tarnished. This greatly shortens their service life resulting in an increase of cost-in-use and wastage of resources. To solve these problems, tremendous efforts have been devoted to improving the wood properties by surface modification. Among the studied techniques, using photocatalyst like TiO_2 [9], ZnO [10–12], CeO_2 [13], and their metal adulterants to functionalize wood surface could endow wood product with several specific functions such as self-cleaning [14], UV-resistance [15], and antibacterial activity [16] via establishing organic-inorganic composite structures.

However, all the traditional photocatalysts are metallic oxides, whose usage can cause heavy metal pollution risks. Additionally, their syntheses involve several complex

✉ Gang Song
songgang@zzu.edu.cn

✉ Zhanhu Guo
zguo10@utk.edu

1 Key Lab of Bio-Based Material Science and Technology (Ministry of Education), College of Material Science and Engineering, Northeast Forestry University, Harbin 150040, China

2 Integrated Composites Laboratory (ICL), Department of Chemical and Biomolecular Engineering, University of Tennessee, TN, Knoxville 37996, USA

3 Advanced Materials Processing Division, Engineered Multifunctional (EMC) Nanotech. LLC, TN, Knoxville 37934, USA

4 Key Laboratory of Materials Processing and Mold (Zhengzhou University), Ministry of Education, National Engineering Research Center for Advanced Polymer Processing Technology, Zhengzhou University, Zhengzhou 450001, China

processes. To address these issues, a method of using graphitic carbon nitride (g-C_3N_4) as novel metal-free photocatalysts has been reported to modify the wood surface with UV protection function [17]. The g-C_3N_4 has a larger band gap of 2.7 eV, higher electron-hole recombination rate, and improved stability than traditional photocatalyst [18–20]. The heterobinding strength between wood surface and g-C_3N_4 was insufficient by our reported hydrothermal method [17]. This resulted in the g-C_3N_4 functional coating being easily peeled off during outdoor use.

In response to this problem, in this work, the g-C_3N_4 was grafted onto the wood surface through the chemical crosslinking method. By forming chemical bonds, the g-C_3N_4 functional coating was firmly immobilized on the wood surface. The properties of the g-C_3N_4-treated wood (GW), including photodegradation, hydrophobic performance, stability of immobilization, and UV resistance ability, were studied and analyzed.

2 Experimental

2.1 Materials

Wood chips (20 mm longitudinal × 20 mm tangential × 5 mm radial) were obtained from sapwood sections of poplar wood (*Populus ussuriensis* Kom from Jiaozuo state forest farm in Henan province). The chips were ultrasonically rinsed in deionized water for 10 min and dried under vacuum at 60 °C till absolute dry; then, we got the original wood (OW). Melamine ($C_3N_3(NH_2)_3$, 99.5%), glutaraldehyde ($C_5H_8O_2$, 50%), 3-aminopropyltriethoxysilane (APTES, 98%), and methyl orange (MO, 96%) were supplied by Tianjin Guangfu Fine Chemical Research Institute and used without further purification. Deionized water was used throughout the study.

2.2 Immobilization of g-C_3N_4 on wood surface

First, g-C_3N_4 powders were synthesized by direct heating of melamine according to previous reports [21]. Briefly, a certain amount of melamine powder was then placed in a covered semi-closed quartz crucible subjected to heat treatment at 550 °C for 2 h at a heating rate of 10 °C/min. After cooling to room temperature, the obtained yellow agglomerates were ground to powder. Then, the powder was then dispersed in water for ultrasonic treatment for 2 h. Finally, the amino-reserved g-C_3N_4 were obtained. In particular, in the typical carbon nitride preparation process, the acid treatment to preserve some amino groups was not used. To make it clear, all the g-C_3N_4 mentioned below were amino-reserved g-C_3N_4.

The g-C_3N_4 was then immobilized on wood surfaces through the chemical cross-linking method. The wood surfaces (tangential) were treated by APTES, where 0.5 mL of APTES (98%) was sprayed on the wood surface by ultrasonic nebulizer. After 5 min reaction, the wood surface was washed three times with deionized water (20 mL) to remove unreacted APTES then dried in air at room temperature. Next, 0.5 mL glutaraldehyde (10% *v*/*v*) was titrated on earlier-treated wood. After several seconds' reaction, the surface was washed three times with deionized water (20 mL) to remove excessive glutaraldehyde. Afterwards, 20 mg g-C_3N_4 was dispersed in 100 mL of deionized water to form suspensions under high-frequency ultrasounds and vigorous magnetic stirring for 2 h. The modified wood surfaces were finally soaked in water phase suspension containing g-C_3N_4 for 10 min. The obtained specimens were washed with deionized water and dried in a vacuum oven at 60 °C for 2 h. Thus, the g-C_3N_4 was grafted on the wood surface. The immobilization amount of g-C_3N_4 was calculated as weight gain (WG) of wood samples from the following equation:

$$\mathrm{WG} = M - M_0 \tag{1}$$

where M is the weight of modified wood and M_0 is the weight of wood chips before any treatment.

2.3 Surface wettability and UV resistance test

The wettability of wood surface before and after treatment was evaluated by exploring water contact angle through a sessile drop on the specimen. The photostabilities of treated wood surfaces were assessed with the UV Weathering Tester (LZW-050A, Yi Heng instruments, Shanghai) at 35 °C and 50% relative humidity (RH). The specimens were exposed for 360 h and then removed from the UV Weathering Tester after an interval of 72 h. Next, they were analyzed for color changes to evaluate the UV resistance properties. The color changes were assessed by a CIELAB system by a portable spectrophotometer (NF333, Mekaster, Beijing). The L^*, a^*, and b^* parameters in CIELAB system were measured three times at each measuring location and the average values were considered for statistical analysis. In CIELAB system, L^* represents lightness, and a^* and b^* are chromaticity coordinates. ΔL^*, Δa^*, and Δb^* values were calculated from the differences between the final and initial values of L^*, a^*, and b^*, respectively. These values were used to estimate the overall color change (ΔE^*), according to Eq. (2):

$$\Delta E^* = \sqrt{\Delta L^{*2} + \Delta a^{*2} + \Delta b^{*2}} \tag{2}$$

The ΔL^*, Δa^*, and Δb^* values provided in Eq. (1) present the changes in L^*, a^*, and b^* parameters, representing the differences between final and initial values.

2.4 Photocatalytic activity tests

The self-cleaning property was evaluated by photocatalytic activity tests. The photocatalytic activities of prepared g-C_3N_4 and modified wood samples were tested by photodegradation of methyl orange in aqueous solutions. The tests were performed under a simulated solar light using photochemical reaction instrument. The light irradiation system combined a 300 W Xe lamp with water circulation cooler to eliminate the temperature effect. The wood specimens were dipped in MO aqueous solution (100 mL, 10 mg/L) subjected to magnetic stirring. To compare the photocatalytic efficiencies between free and modified woods with g-C_3N_4, the immobilization amount with g-C_3N_4 on wood surface was calculated as weight gain (WG). g-C_3N_4 powder with the same amount of WG was then dispersed in an MO aqueous solution (100 mL, 10 mg/L) and stirred for 1 h in the dark to reach an adsorption-desorption equilibrium before irradiation. At given time intervals, 5-mL samples were taken from the reaction suspension, centrifuged, filtered off, and then subjected to spectrophotometrical determination of MO concentration.

2.5 Stability of immobilization

The stability of immobilization is an important parameter of the modified process that determines the efficiency and cost performance in further applications. The stability was determined by measuring the remaining content of g-C_3N_4 after recycling photocatalytic activity tests.

The remaining content of g-C_3N_4 is calculated from Eq. (3):

$$R(\%) = \frac{M' - M_0}{WG} \times 100 \tag{3}$$

where R is the remained content of the g-C_3N_4 (%), M' is the weight of the modified wood after a certain photocatalytic activity tests, M_0 is the weight of original wood (g), and WG is the same quantity as in Eq. (1). And the GW prepared with our reported hydrothermal method was tested as control group [17].

2.6 Characterization

X-ray diffraction (XRD, D/max 2200, Rigaku, Japan) with Cu-Kα radiation ($\lambda = 0.15406$ nm) was performed at 40 kV and 30 mA in the 2θ range from 5 to 60° at scan rate of 5° min^{-1}. The morphologies of wood surfaces were observed through field emission scanning electron microscopy (SEM, JSM-7500F, JEOL, Japan) operating at 5 kV in combination with EDS. The specimens prepared for SEM were coated with a thin layer of gold before visualization. The C/N ratios of the specimens were determined by elemental analysis performed with an elemental analyzer (Euro Vector EA3000, Italy). The experimental error in weighing was set to ±0.001 mg. The Fourier transform infrared spectra (FTIR) in 4000–400 cm^{-1} region were recorded on Nicolet IS10. Optical properties of g-C_3N_4 were characterized by UV-Vis diffuse reflectance spectroscopy (UV-Vis DRS, Beijing Purkinje TU-190, China) equipped with an integrated sphere attachment and $BaSO_4$ as reference.

3 Results and discussion

3.1 Characterization

The amino-reserved g-C_3N_4 was characterized by XRD (Fig. 1a) and FTIR (Fig. 1b) analyses. Figure 1a clearly shows two distinct peaks in g-C_3N_4 profile. The stronger peak at 2θ = 27.3° was assigned to the (002) crystal planes, originating from the periodic stacking of layers inside the g-C_3N_4 stratified structure. The low-angle peak at 2θ = 13.1° with an interplanar distance of 0.76 nm was indexed to (100) and associated with inter-layer stacking. No other reflection peaks were found, consistent with previous reports [19]. As shown in Fig. 1b, several strong absorption peaks were observed in the range of 1200~1650 cm^{-1}, attributed to the typical stretching modes of CN heterocycles. The sharp peak at 1625 cm^{-1} was associated with good crystallinity of g-C_3N_4. Additionally, the sharp peak at 801 cm^{-1} would belong to triazine ring mode. The broad peaks between 3000 and 3300 cm^{-1} were attributed to the stretching vibration of N–H bonds (–NH_2 or –NH–) [22].

The changes in the surface chemical groups of wood samples during the chemical cross-linking treatment were investigated by FTIR analyses. Typical bands of OW assigned to cellulose were located at 2931 and 2862 cm^{-1} for the C–H stretching vibrations of, respectively, CH_3 and CH_2 groups existing throughout the modification. The broad band at 3342 cm^{-1} corresponded to the O–H stretching vibration in OW (Fig. 2a) [23]. After treatment with APTES, the band with similar wavenumbers that appeared in the amino-functionalized wood underwent weakening (Fig. 2b). The latter could be attributed to the reaction between hydroxyl groups on wood surface and ethoxyl groups of APTES, resulting in reduced hydroxyl groups and appearance of N–H stretching vibration at 3400 cm^{-1}. The bands at 1730, 1595, and 1512 cm^{-1} were assigned to the C=O stretching vibrations, aromatic chain of lignin, and side chain carbonyl C=O, respectively. Those at 1416, 1310, and 1240 cm^{-1} were attributed to the C–H bending mode, O–H bending mode, and C–O stretching mode, respectively. The intensities of the absorption peaks at wavenumbers between 1000 and 2000 cm^{-1} were weakened after modification and could be

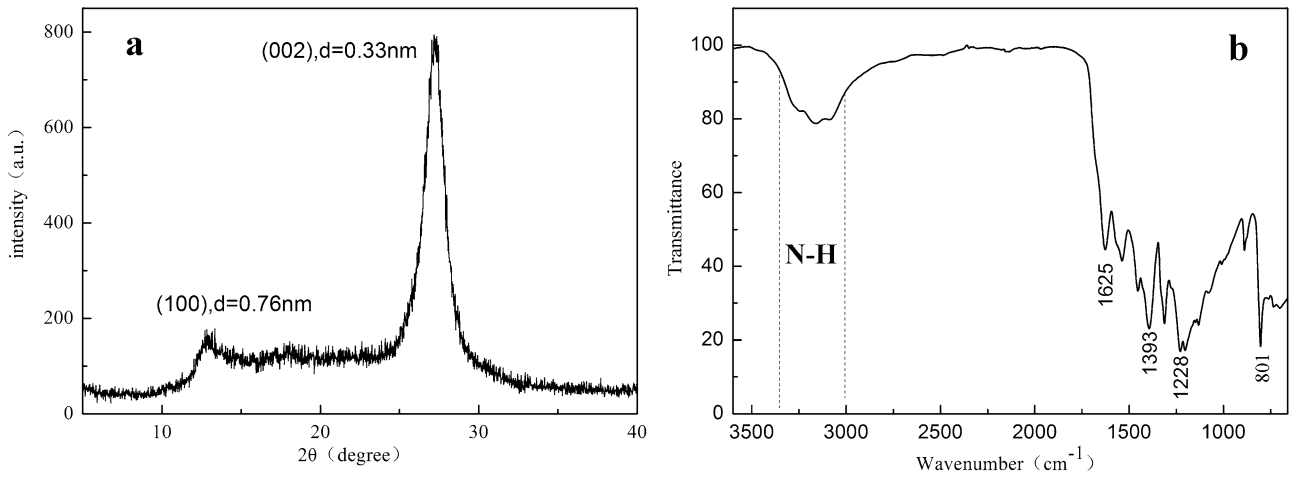

Fig. 1 XRD pattern (**a**) and FTIR spectra (**b**) of g-C_3N_4

attributed to the coverage of wood surface with APTES. No clear differences were noticed between amino-functionalized wood and GW (Fig. 2c), possibly due to the low content of g-C_3N_4 on wood surface.

The surface morphologies of the specimens were observed by SEM. The tangential section of OW showed typical pits structures with clear and smooth surface (Fig. 3a). After chemical cross-linking modification, the pits of OW were coated with dense g-C_3N_4 (Fig. 3b), making the GW surface rougher. Typical laminar morphology structure of g-C_3N_4 can clearly be seen in the magnified image of Fig. 3c. The surface elemental compositions of treated woods were determined by energy-dispersive X-ray spectroscopy (EDS) (Fig. 3d). Both nitrogen and silicon barely existed on OW surface, hence should come from reacted grafted APTES.

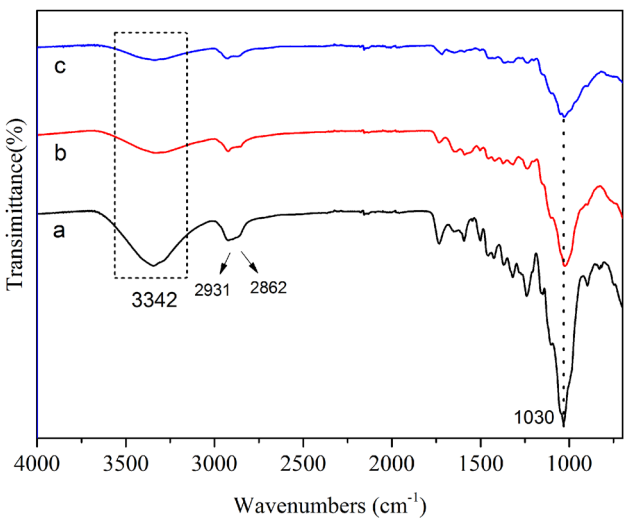

Fig. 2 FTIR spectra of OW (**a**), amino-functionalized wood (**b**), and GW (**c**)

The N/Si atom ratio was estimated to be 1.61, which was higher than that of APTES (1.0). The increase in nitrogen atoms should originate from cross-linked g-C_3N_4. The carbon and oxygen would originate from wood, APTES, and glutaraldehyde. No other elements were detected. Overall, the EDS results further confirmed the presence of g-C_3N_4 on wood surface. According to the weight gain of wood sample, the grafting density of g-C_3N_4 was 1~2 mg/cm^2.

3.2 Mechanism of chemical cross-linking

The mechanism of chemical cross-linking is proposed in Fig. 4. There are many hydroxyl groups on wood surface, which belong to cellulose, hemicellulose, and lignin. The cross-linking process could be described by three consecutive steps. First, the wood surface was amino-functionalized by APTES through condensation reaction between the hydroxyl groups of wood surface and ethoxyl groups of APTES. Second, glutaraldehyde as a cross-linking agent with aldehyde groups at both ends of the carbon chain could react with the amino groups. The Schiff base condensations between the aldehyde groups of glutaraldehyde and amino groups of amino-functionalized wood grafted the aldehyde on wood surface. Third, the amino groups in g-C_3N_4 were cross-linked on wood surface through the Schiff base condensation again [24, 25].

3.3 Surface properties

Figure 5 shows the UV-Vis absorption spectra of GW. High absorbance reaching 90% was observed with GW in the region 280~400 nm, meaning that 90% UVA (400~315 nm UV region) and UVB (315~280 nm region) were absorbed by g-C_3N_4 coating. As the wavelength was decreased from 280 to 200 nm, the absorbance

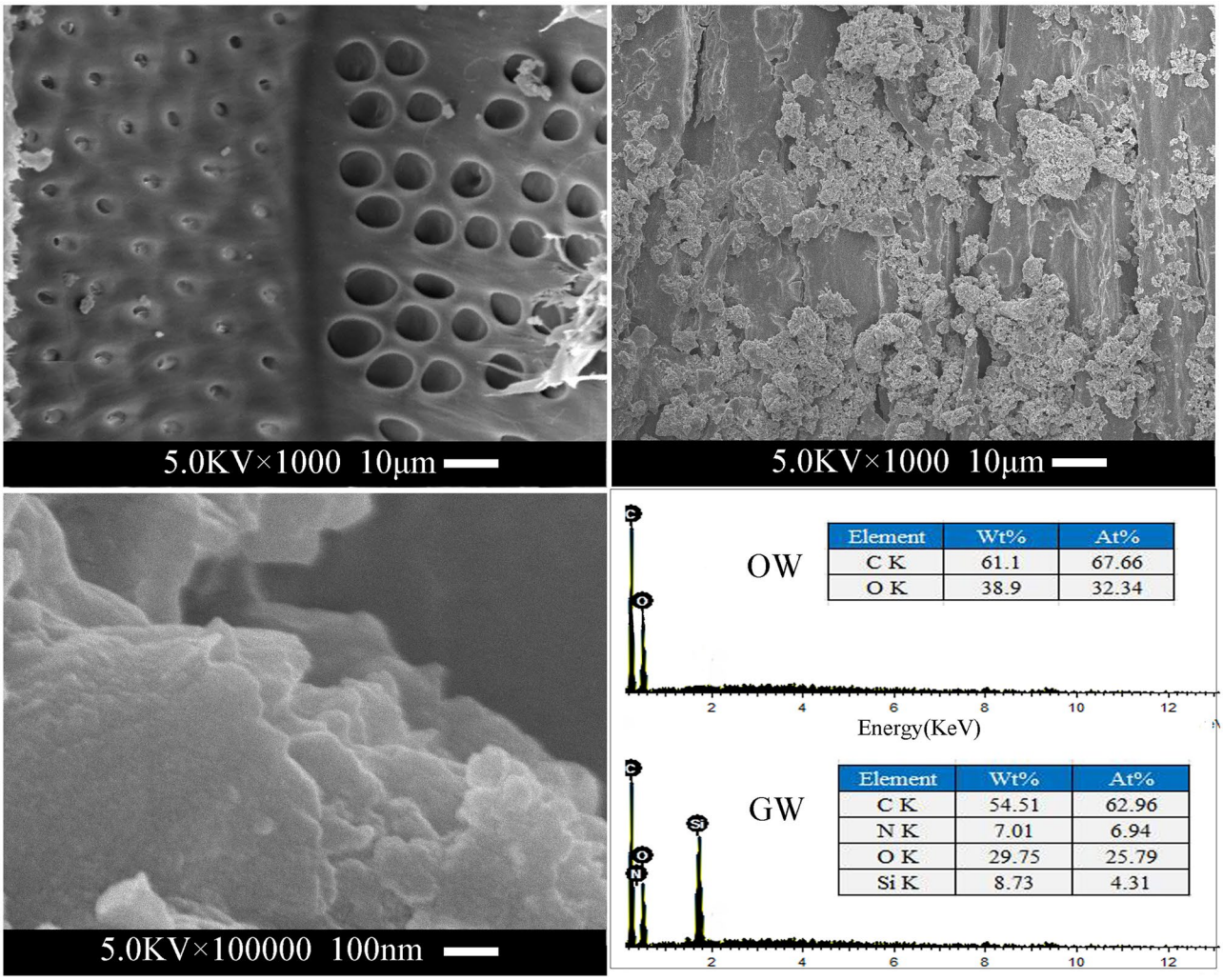

Fig. 3 SEM images of OW (**a**) and GW (**b**, **c**). EDS of OW and GW. The insets show the corresponding mass and atomic proportions of the elements, respectively (**d**)

became much lower [26, 27]. The wavelengths in 280~100 nm range corresponded to the UVC radiation, which was completely absorbed by the ozone layer and atmosphere. Also, the visible region (400~800 nm) would hardly cause damage to wood. Thus, the wood surface could well be protected from UV degradation through g-C_3N_4 coating.

Figure 6 shows the photographs of OW and GW after 15-day accelerated weathering tests. The OW exposed under the UV lights had a significant discoloration from off white to light yellow. However, CW did not show any obvious visible discoloration.

Figure 7 presents the overall color change (ΔE^*) tendencies of the OW and GW after UV resistance tests. The color

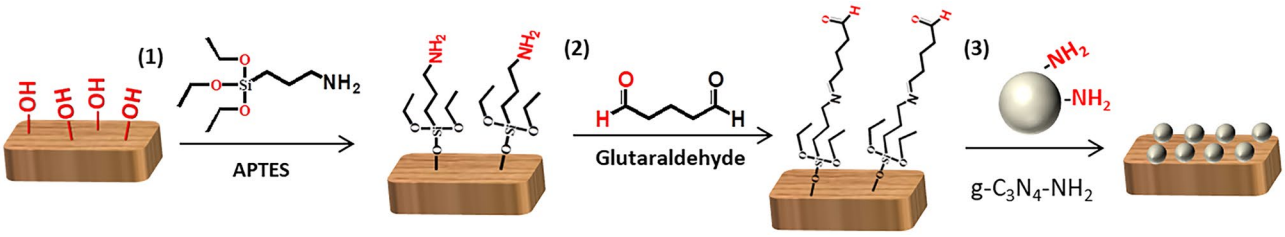

Fig. 4 Mechanism of chemical cross-linking

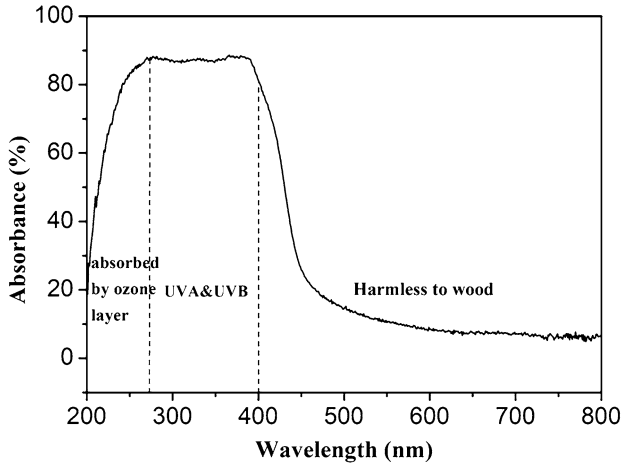

Fig. 5 UV–Vis absorption spectra of GW

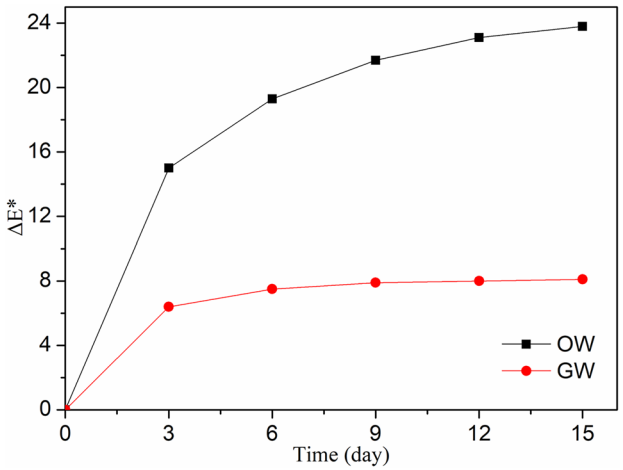

Fig. 7 ΔE* of the OW and GW for every 3 days

changed quickly in the first 3 days and slowed down gradually. According to the UV-Vis absorption spectra of g-C_3N_4, the solar radiation between 250 and 420 nm was mostly absorbed by g-C_3N_4 immobilized on the wood surface resulting in smaller color changes. The total color change of GW was much smaller, indicative of lesser lignin damage. These findings further confirmed the UV resistance properties of g-C_3N_4 coatings [28].

The self-cleaning property was evaluated by photocatalytic performance tests. Figure 8 presents the photodegradation efficiencies of free g-C_3N_4, OW, and GW. OW illustrated no photocatalytic activity. GW exhibited a photocatalytic activity, but the photodegradation efficiency declined gradually. This could result from the decrease in the solution concentration. Compared with free g-C_3N_4, GW showed a lower photocatalytic activity probably due to the restriction in reaction areas of g-C_3N_4 in solution after cross-linking on wood surface. The endowing of wood surface with photocatalyst properties of g-C_3N_4 further confirmed the successful cross-linking of g-C_3N_4 on wood surface.

Wood surface is susceptible to water erosion, so its surface hydrophobicity is important. Figure 9 shows the water contact angle (WCA) of the OW and GW. The OW surface appears as hydrophilic with WCA of 55.1° (Fig. 9a). After being modified by g-C_3N_4, the hydrophobicity of the surface got enhanced as the WAC increased to 78.5° (Fig. 9b). According to the FTIR results, these results could be attributed to the decrease of hydrophilic groups (–OH) on wood surface. In addition, the hydrophilic interaction of amino is weaker than the hydrophobic effect of hydroxyl groups,

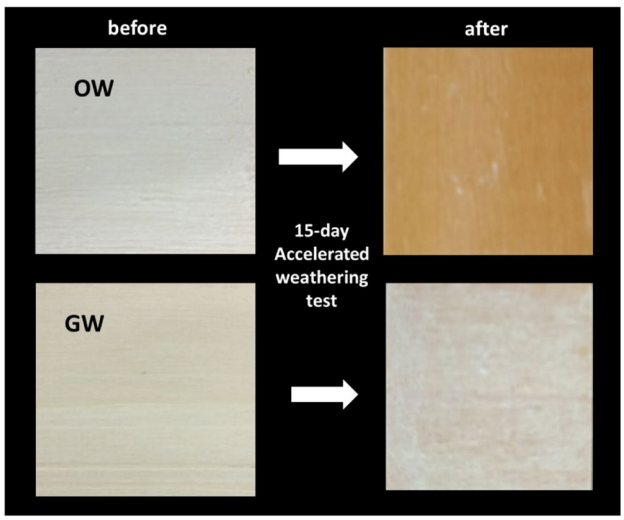

Fig. 6 Photographs of OW and GW, before and after accelerated weathering test

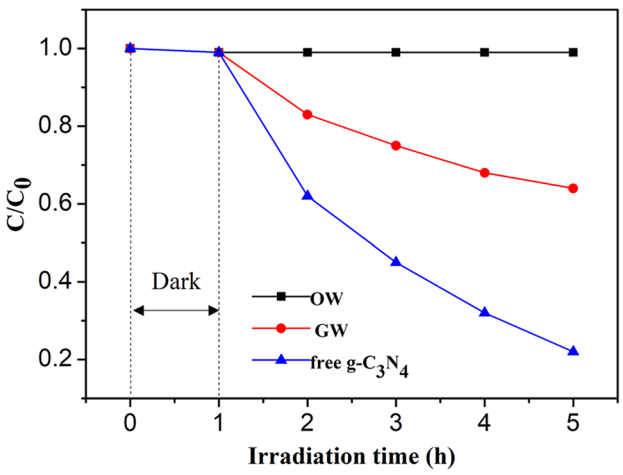

Fig. 8 Photodegradation of methyl orange over free g-C_3N_4, OW, and GW

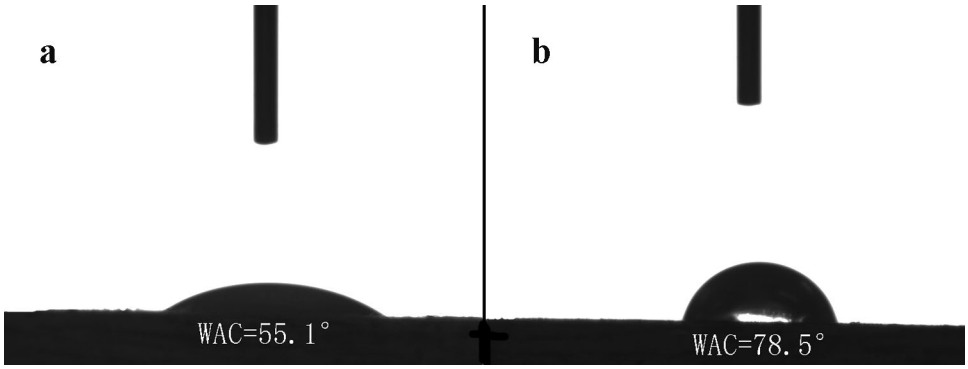

Fig. 9 WCA of the OW (**a**) and GW (**b**)

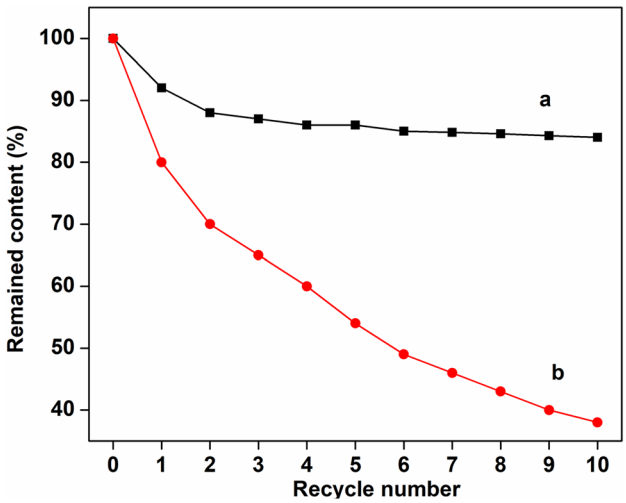

Fig. 10 Remained content of g-C_3N_4 of the GW prepared with chemical crosslinking method (**a**) and hydrothermal method (**b**)

which led to a significant increase in the hydrophobicity of wood surface.

The stability of immobilization was evaluated by the remained content of g-C_3N_4 (Fig. 10). After recycling photocatalytic activity tests, the remained content of g-C_3N_4 is stable at 84% which is much higher than the control group (our reported hydrothermal method).

The stability of immobilization was evaluated by the remained content of g-C_3N_4 (Fig. 10). After recycling photocatalytic activity tests, the remained content of g-C_3N_4 is stable at 84% which is much higher than the control group (our reported hydrothermal method).

4 Conclusions

A method of preparing g-C_3N_4-modifiedfunctional wood by chemical crosslinking has been proposed. Through Schiff basecondensation reactions, the g-C_3N_4 was firmly grafted onwood surface. FTIR, XRD, SEM, and EDS analysesindicated successful chemical cross-linking treatment. The UV-Vis spectra of GW achieved about 85%absorption of UVA and UVB lights by the coating. After 15days of acceleratedweathering tests, the total color change (ΔE^*)of GW reached only ~8%, which was muchless than that of OW (~24%). After 10 cycles of photocatalytic activity tests, the remained contentof g-C_3N_4 was stable at 84%, which was much higher thanthe 40% of control group. In addition, the WCA of wood surface was improved from 55.1° to 78.5°, which could be conduciveto the improvement of weather resistance property. Overall, this developed GWis promising as self-cleaning, UV resistant, and high-value-added wood product.

Funding The authors received financial support from The National Natural Science Fundation of China (31971587) and Special Project for Double First-Class—Cultivation of Innovative Talents (No.000/41113102).

Declarations

Conflict of interest The authors declare that they have no conflict of interest.

References

1. Liao H, Zhang B, Huang L, Ma D, Jiao Z, Xie Y, Tan S, Cai X (2015) The utilization of carbon nitride to reinforce the mechanical and thermal properties of UV-curable waterborne polyurethane acrylate coatings. Prog Org Coat 89:35–41. https://doi.org/10.1016/j.porgcoat.2015.07.021
2. Nikolic M, Lawther JM, Sanadi AR (2015) Use of nanofillers in wood coatings: a scientific review. J Coat Technol Res 12(3):445–461. https://doi.org/10.1007/s11998-015-9659-2
3. Lin C-M (2015) Functional composite metal for WC-dispersed 304L stainless steel matrix composite with alloying by direct laser: microstructure, hardness and fracture toughness. Vacuum 121:96–104. https://doi.org/10.1016/j.vacuum.2015.07.023
4. Wang Y, Xie W, Liu H, Gu H (2020) Hyperelastic magnetic reduced graphene oxide three-dimensional framework with superb oil and organic solvent adsorption capability. Advanced Composites and Hybrid Materials:1–12. https://doi.org/10.1007/s42114-020-00191-z

5. Xie W, Shi Y, Wang Y, Zheng Y, Guo Z (2020) Electrospun iron/cobalt alloy nanoparticles on carbon nanofibers towards exhaustive electrocatalytic degradation of tetracycline in wastewater. Chem Eng J:126585. https://doi.org/10.1016/j.cej.2020.126585
6. Cai J, Tian J, Gu H, Guo Z (2019) Amino carbon nanotube modified reduced graphene oxide aerogel for oil/water separation. ES Materials & Manufacturing 6:68–74. https://doi.org/10.30919/esmm5f611
7. Gu H, Zhou X, Lyu S, Pan D, Guo Z (2019) Magnetic nanocellulose-magnetite aerogel for easy oil adsorption. J Colloid Interface Sci 560:849–856. https://doi.org/10.1016/j.jcis.2019.10.084
8. Xz A, Qf B, Hl C, Hg A, Zg D (2021) Solvent-free nanoalumina loaded nanocellulose aerogel for efficient oil and organic solvent adsorption. J Colloid Interface Sci 581:299–306. https://doi.org/10.1016/j.jcis.2020.07.099
9. Luo L, Yang Y, Xiao M, Bian L, Yuan B, Liu Y, Jiang F, Pan X (2015) A novel biotemplated synthesis of TiO2/wood charcoal composites for synergistic removal of bisphenol A by adsorption and photocatalytic degradation. Chem Eng J 262:1275–1283. https://doi.org/10.1016/j.cej.2014.10.087
10. Dong Y, Yan Y, Ma H, Zhang S, Li J, Xia C, Shi SQ, Cai L (2017) In-situ chemosynthesis of ZnO nanoparticles to endow wood with antibacterial and UV-resistance properties. J Mater Sci Technol 33(3):266–270. https://doi.org/10.1016/j.jmst.2016.03.018
11. Guo H, Fuchs P, Cabane E, Michen B, Hagendorfer H, Romanyuk YE, Burgert I (2016) UV-protection of wood surfaces by controlled morphology fine-tuning of ZnO nanostructures. Holzforschung 70(8):699–708. https://doi.org/10.1515/hf-2015-0185
12. Sun Q, Lu Y, Zhang H, Yang D, Wang Y, Xu J, Tu J, Liu Y, Li J (2012) Improved UV resistance in wood through the hydrothermal growth of highly ordered ZnO nanorod arrays. J Mater Sci 47(10):4457–4462. https://doi.org/10.1007/s10853-012-6304-7
13. Auffan M, Masion A, Labille J, Diot M-A, Liu W, Olivi L, Proux O, Ziarelli F, Chaurand P, Geantet C (2014) Long-term aging of a CeO2 based nanocomposite used for wood protection. Environ Pollut 188:1–7. https://doi.org/10.1016/j.envpol.2014.01.016
14. Sheng C, Wang C, Wang H, Jin C, Sun Q, Li S (2017) Self-photodegradation of formaldehyde under visible-light by solid wood modified via nanostructured Fe-doped WO3 accompanied with superior dimensional stability. J Hazard Mater 328:127–139. https://doi.org/10.1016/j.jhazmat.2017.01.018
15. Aloui F, Ahajji A, Irmouli Y, George B, Charrier B, Merlin A (2007) Inorganic UV absorbers for the photostabilisation of wood-clearcoating systems: comparison with organic UV absorbers. Appl Surf Sci 253(8):3737–3745. https://doi.org/10.1016/j.apsusc.2006.08.029
16. Guo H, Bachtiar EV, Ribera J, Heeb M, Schwarze FWMR, Burgert I (2018) Non-biocidal preservation of wood against brown-rot fungi with a TiO 2/Ce xerogel. Green Chem 20(6):1375–1382. https://doi.org/10.1039/C7GC03751A
17. Yuan B, Ji X, Nguyen TT, Huang Z, Guo M (2019) UV protection of wood surfaces by graphitic carbon nitride nanosheets. Appl Surf Sci 467:1070–1075. https://doi.org/10.1016/j.apsusc.2018.10.251
18. Christoforidis KC, Montini T, Bontempi E, Zafeiratos S, Jaén JJD, Fornasiero P (2016) Synthesis and photocatalytic application of visible-light active β-Fe2O3/g-C3N4 hybrid nanocomposites. Appl Catal B 187:171–180. https://doi.org/10.1016/j.apcatb.2016.01.013
19. Wang X, Maeda K, Thomas A, Takanabe K, Xin G, Carlsson JM, Domen K, Antonietti M (2009) A metal-free polymeric photocatalyst for hydrogen production from water under visible light. Nat Mater 8(1):76–80. https://doi.org/10.1038/nmat2317
20. Wen J, Xie J, Chen X, Li X (2017) A review on g-C3N4-based photocatalysts. Appl Surf Sci 391:72–123. https://doi.org/10.1016/j.apsusc.2016.07.030
21. Li X, Zhang J, Shen L, Ma Y, Lei W, Cui Q, Zou G (2009) Preparation and characterization of graphitic carbon nitride through pyrolysis of melamine. Appl Phys A 94(2):387–392. https://doi.org/10.1007/s00339-008-4816-4
22. Niu P, Zhang L, Liu G, Cheng HM (2012) Graphene-like carbon nitride nanosheets for improved photocatalytic activities. Adv Funct Mater 22(22):4763–4770. https://doi.org/10.1002/adfm.201200922
23. Olsson SK, Johansson M, Westin M, Östmark E (2014) Reactive UV-absorber and epoxy functionalized soybean oil for enhanced UV-protection of clear coated wood. Polym Degrad Stab 110:405–414. https://doi.org/10.1016/j.polymdegradstab.2014.09.017
24. Hu J, Yuan B, Zhang Y, Guo M (2015) Immobilization of laccase on magnetic silica nanoparticles and its application in the oxidation of guaiacol, a phenolic lignin model compound. RSC advances 5(120):99439–99447. https://doi.org/10.1039/c5ra14982g
25. Chen M, Liu C (2017) Preparation, characterization and properties of fiber reinforced composites using silicon-containing hybrid polymers. Polym Adv Technol 28(2):145–151. https://doi.org/10.1002/pat.3868
26. Wan C, Jiao Y, Li J (2015) In situ deposition of graphene nanosheets on wood surface by one-pot hydrothermal method for enhanced UV-resistant ability. Appl Surf Sci 347:891–897. https://doi.org/10.1016/j.apsusc.2015.04.178
27. Schaller C, Rogez D (2007) New approaches in wood coating stabilization. J Coat Technol Res 4(4):401–409. https://doi.org/10.1007/s11998-007-9049-5
28. Rosu D, Teaca C-A, Bodirlau R, Rosu L (2010) FTIR and color change of the modified wood as a result of artificial light irradiation. J Photochem Photobiol, B 99(3):144–149. https://doi.org/10.1016/j.jphotobiol.2010.03.010